The energy requirements of ion homeostasis determine the lifespan of starving bacteria

Severin Schink[1, #], Mark Polk[1], Edward Athaide[1], Avik Mukherjee[1], Constantin Ammar[1,2], Xili Liu[1], Seungeun Oh[1], Yu-Fang Chang[1], and Markus Basan[1, #]

[1] Systems Biology Department, Harvard Medical School, 200 Longwood Ave, 02115 MA, USA

[2] Department of Informatics, Ludwig-Maximilians-Universität München, Amalienstrasse 17, 80333 München, Germany

[#] Correspondence: severin_schink@hms.harvard.edu and markus@hms.harvard.edu

Abstract

The majority of microbes on earth, whether they live in the ocean, the soil or in animals, are not growing, but instead struggling to survive starvation[1–6]. Some genes and environmental conditions affecting starvation survival have been identified[7–13], but despite almost a century of study[14–16], we do not know which processes lead to irreversible loss of viability, which maintenance processes counteract them and how lifespan is determined from the balance of these opposing processes. Here, we used time-lapse microscopy to capture and characterize the cell death process of *E. coli* during carbon starvation for the first time. We found that a lack of nutrients results in the collapse of ion homeostasis, triggering a positive-feedback cascade of osmotic swelling and membrane permeabilization that ultimately results in lysis. Based on these findings, we hypothesized that ion transport is the major energetic requirement for starving cells and the primary determinant of the timing of lysis. We therefore developed a mathematical model that integrates ion homeostasis and 'cannibalistic' nutrient recycling from perished cells[16,17] to predict lifespan changes under diverse conditions, such as changes of cell size, medium composition, and prior growth conditions. Guided by model predictions, we found that cell death during starvation could be dramatically slowed by replacing inorganic ions from the medium with a non-permeating osmoprotectant, removing the cost of ion homeostasis and preventing lysis. Our quantitative and predictive model explains how survival kinetics are determined in starvation and elucidates the mechanistic underpinnings of starvation survival.

Results

Starving microbes undergo a gradual decrease in viability that can resemble exponential decay [2,14,15,17–20]. While the rate and specific dynamics of the initial decay can depend on the type of starvation (Fig. S1A) and on the organism (Fig S1B), the overall phenotype of exponential decay is remarkably conserved.

To uncover the molecular mechanisms underlying this universal phenomenon, we focused on the exponential decay of viability of *Escherichia coli* K-12 in carbon starvation, where cultures lose about 99.9% of viability within 10 days (Fig. 1A). We first asked which biosynthetic processes are important for starvation survival. We measured survival dynamics in batch, while inhibiting several major cellular biosynthetic processes with different antibiotics (Fig. 1B). Strikingly, the only treatment that led to an accelerated decrease in viability and eventually extinction of the culture was the inhibition of fatty acid synthesis with cerulenin, indicating a role of the plasma membrane in starvation survival.

To determine the causes of loss of viability in starvation, we imaged individual bacteria during starvation with live-cell, time-lapse microscopy, using a membrane potential dye as a readout for ion homeostasis; see Methods. We found that within a few hours after nutrient depletion, the cytoplasm of *E. coli* contracted and detached from the cell wall at the poles (Fig. 1C, image at 16 h; Fig. S2A&B - quantification and statistics, Fig. S2C&D - SEM & TEM), a process called plasmolysis that is typical for bacteria in starvation[18,21]. By continuing to track starving bacteria for seven days, we captured the death process in thousands of bacteria: spontaneous depolarization of the cytoplasm was rapidly followed by swelling and lysis (Fig. 1C, 26 h & 26.3 h; Fig. 1D). Swelling of the cytoplasm led to stretching of the cell envelope, indicated by an increase in cell length (Fig. 1E, Fig. S2E&F), and lysis led to a sudden loss of biomass (Fig. 1F, Fig. S2G&H). Analyzing the succession of events, we found that the collapse of membrane potential coincided with cytoplasmic expansion (-0.05±0.50 h, Fig. S2F) and preceded lysis (2.0±1.4 h, Fig. S2H). This led us to hypothesize that the uncontrolled expansion is caused by a catastrophic failure of ion homeostasis, resulting in a build-up of osmotic pressure and eventually lysis. We next stained bacteria with propidium iodide (PI), a non-toxic stain (Fig. S3A) that intercalates irreversibly with
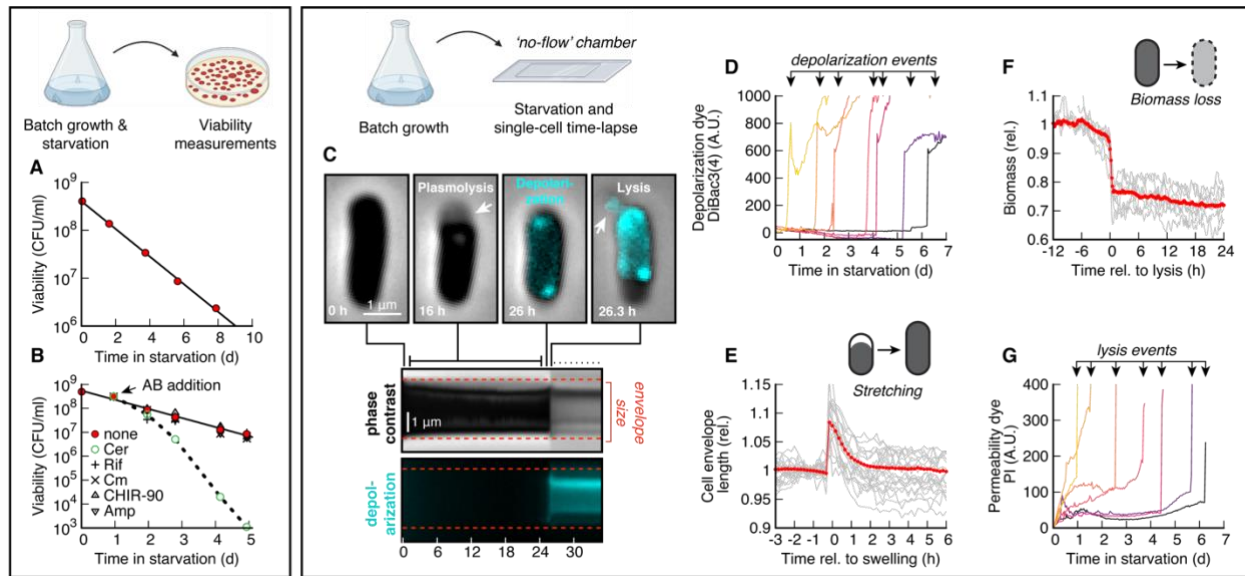
2

Figure 1. Survival dynamics of *E. coli* in carbon starvation. (**A**) Viability of *E. coli* K-12 NCM3722 in N+C- minimal medium (batch). Growth medium supplemented with 0.1% glucose; starvation induced by medium switch; viability measured in colony forming units (CFU/ml) (Methods). Line: Exponential fit. Data points are an average of n=3 replicates. (**B**) Viability of control (red) compared to cerulenin (Cer, fatty acid synthesis), rifaximin (Rif, transcription), chloramphenicol (Cm, translation), CHIR-90 (lipid-A synthesis) and ampicillin (Amp, cell wall synthesis). Antibiotics were added daily, starting at 24 h at 10x MIC. Data points are an average of n=3 replicates. (**C**) Live-cell imaging of *E. coli* in a 'no-flow' chamber (Methods). Plasmolysis, the retraction of cytoplasmic membrane from cell envelope, lasted from the first hours of starvation until shortly before death (see Kymograph). During plasmolysis, the cytoplasm spontaneously depolarizes (cyan DiBac3(4) signal turns on at 26 h), which coincides with swelling (Fig. S2E&F). Finally, the bacterium lyses ('arrow' at 26.3 h), which is typically delayed from swelling (Fig. S2G-H). Total # of bacteria: 14.498. (**D**) Single cell traces of seven representative bacteria dying on different days show a sudden spike signal, indicating rapid loss of ion homeostasis. (**E**) Cell envelope length of single cells, aligned to time-point of swelling ('grey'; mean in 'red'). # of bacteria: 858. (**F**) Single-cell biomass, measured with quantitative phase microscopy (QPM; Methods) aligned to time-point of lysis. Loss of biomass: 28±7 % (Fig. S2G). # of bacteria: 34. (**G**) Single-cell traces of fluorescence signal of propidium iodide (PI) of the seven cells of panel C. Permeability is measured as the slope of the staining dynamics. See Fig. S4 for combined DiBac3(4) and PI traces of individual bacteria.

62   DNA (Fig. S3B&C), which allows us to use it as a metric for cell permeability (see Fig. S3D, E).

63   We found that PI diffuses through the membrane at a slow rate during starvation, indicating that

64   the membrane is slightly permeable in viable bacteria, but shows a sharp increase when bacteria

65   lyse (Fig. 1G).

66

3

67 To investigate the morphology of the cell envelope, and in particular the inner membrane, we also
68 performed transmission electron micrography (TEM) during starvation survival. Electron
69 microscopy revealed dramatic changes of membrane morphology. While early in starvation there
70 was excess cytoplasmic membrane, after 48 h in starvation the excess material had vanished and
71 the shape of the membrane at the pole was nearly half-spherical, indicating tension on the
72 membrane (Fig. S2C).

73

74 Based on these observations, we hypothesized that maintaining ion homeostasis and membrane
75 integrity are the two most important processes that prevent lysis of starving bacteria. The role of
76 membrane integrity is straightforward to understand, but the role of ion homeostasis is less obvious.
77 However, all cells must actively transport inorganic ions out of their cytoplasm to reduce their
78 internal solute concentration. If this process fails, the excess concentrations of metabolites,
79 macromolecules and counterions inside the cell leads to the influx of water, swelling and lysis[22,23].
80 Therefore, maintaining osmolarity to prevent swelling is a continuous process that consumes
81 energy that is in short supply during starvation. If our hypothesis is correct, this would suggest that
82 maintenance of ion homeostasis is the largest indispensable energy cost of starving cells.

83

84 To test whether these ideas are sufficient to explain the key experimental observations on starving
85 bacterial populations, we devised a simple mathematical model (Fig. 2A). One important goal for
86 the model was to explain how the exponential decay of viability of Fig. 1A emerges from the
87 seemingly random time to death of single cells, as observed in Fig. 1D. The model assumes that
88 ions from the medium (red, coarse-grained into a single species) diffuse into the cytoplasm and
89 are exported using active transport, which consumes energy provided by nutrients (green); see Eq.
90 (1). Nutrients released from dying cells are cannibalized and provide an energy source to surviving
91 cells[16,17]; see Eq. (2). Based on experimental findings[24–26], we also assumed that membrane
92 permeability is increased by membrane tension. Biological fluctuations in permeability and
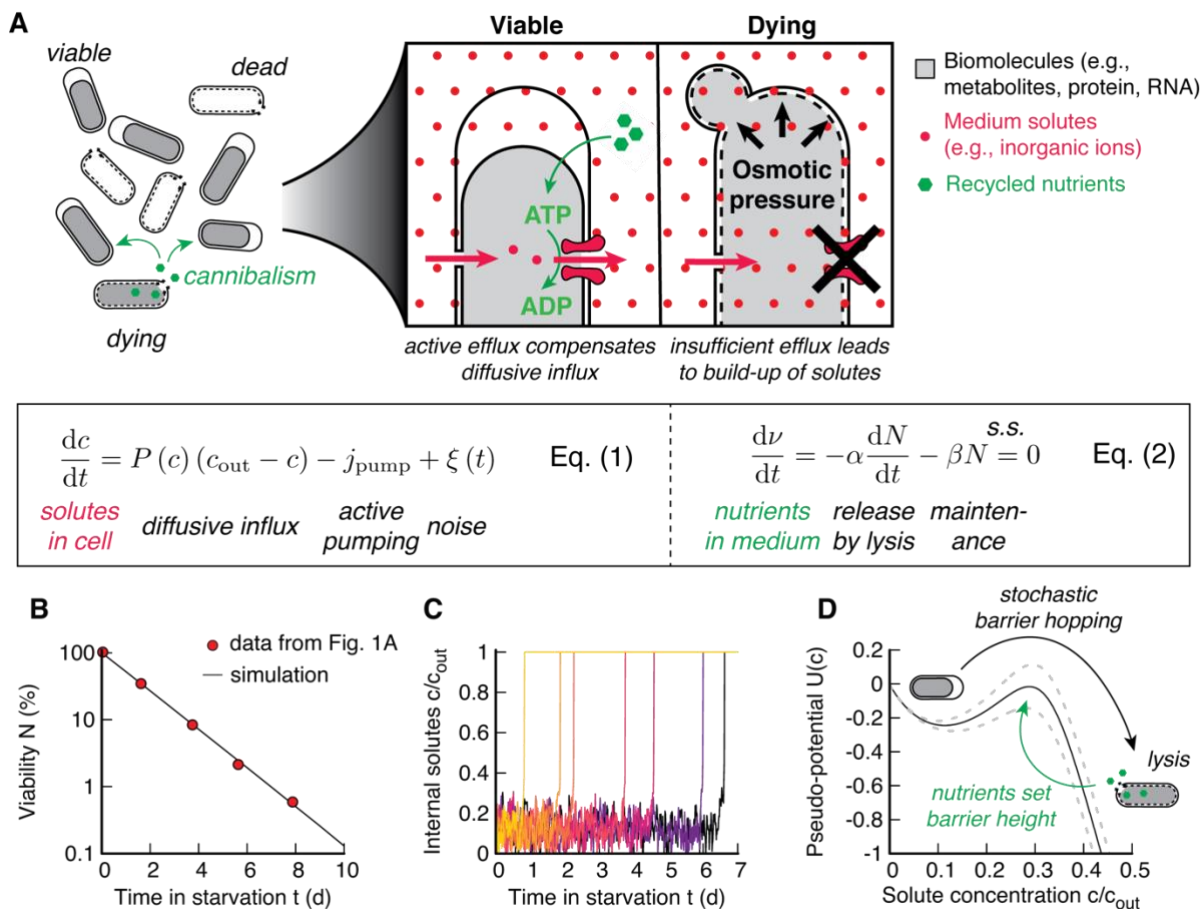93 pumping are integrated in a normal-distributed noise term.

Figure 2. Ion homeostasis maintenance model. (**A**) Nutrients released by lysis are cannibalized by viable bacteria (left) and are used to pump out solutes (e.g., ions) from the cytoplasm to the medium (right). If sufficient nutrients are present to support pumping, then the cytoplasm contracts (plasmolysis) until the concentration of solutes from biomass balances c_{out}. Insufficient pumping leads to collapse of ion gradients, osmotic water inflow and swelling, resulting in lysis. The dynamics of internal solute concentration, c_{in}, (Eq. 1) are given by diffusive influx (Fick's law; permeability P, ion gradient $\Delta c = c_{out} - c_{in}$), active pumping (j_{pump}, which is a part of the total maintenance β), and normal-distributed noise $\xi(t)$. Stretching of the membrane by increased turgor pressure (i.e., decreased Δc) increases $P(\Delta c)$. The dynamics of nutrients in the medium v is given by release of nutrients (recycling yield α), and maintenance β. N is the number of viable bacteria in the culture. In steady state 's.s.', $v = const$. See SI for details on the model. (**B**) Simulated loss of viability of 10^5 bacteria (black line) compared to experimental data from Fig. 1A. (**C**) Dynamics of single-cell solute concentration for bacteria dying at different time-points shows random variations around a small solute concentration, and a spontaneous loss of homeostasis, analog to Fig. 1D. (**D**) The model can be mapped onto a potential $U(c)$, 'black line', with $dc/dt = -U'(c) + \xi(t)$. Height of the barrier self-adjusts. Dashed lines show the effect of a 10% change in death rate on the potential barrier.

94

5

95   Simulations of this 'ion homeostasis' model closely matched experimental observations. Indeed,

96   the model dynamics yielded an exponential decay in viability (Fig. 2B) and a spontaneous loss of

97   ion homeostasis and death (Fig. 2C). This is because in the model, the spontaneous death process

98   can be understood as a stochastic escape from a potential well (Fig. 2D), similar to the classic

99   Kramer's escape model in physics[27]. In the potential well, starving cells are in plasmolysis,

100   minimizing tension on the membrane. But unlike in the classic Kramer's escape model, the

101   potential barrier itself is created by nutrients released from dying cells, i.e., cells that have crossed

102   the potential barrier. This leads to a steady state where most bacteria are supplied with just enough

103   nutrients to remain in the potential well, but the potential barrier remains small enough to let cells

104   to escape the well at a low rate and provide nutrients to support surviving cells. Therefore, because

105   the barrier height itself is set by the escape rate over the barrier, even small fluctuations in the

106   underlying biological variables are sufficient to result in a highly stochastic exponential decay in

107   viability; see SI. This closely resembles our experimental observations, where the vast majority of

108   starving cells remain in plasmolysis (low internal ion concentration), but a subset stochastically

109   undergoes expansion and lysis (ion influx and crossing the potential barrier).

110

111   To experimentally test this model and the ion homeostasis mechanism it describes, we derived a

112   set of quantitative predictions from the model. For bacteria that are in the potential well, the

113   internal ion concentration c_{in} is in steady-state and ion efflux from active transport, j_{out}, is

114   balanced by passive diffusive influx, j_{in}. Fick's law of diffusion states that the diffusive influx j_{in}

115   is proportional to the concentration gradient of ions across the membrane, $j_{\text{in}} = P\Delta c$, where P is

116   the permeability of the membrane and $\Delta c = c_{\text{out}} - c_{\text{in}}$ is the ion gradient. Hence, the energy

117   expenditure of bacteria for pumping ions, denoted by β, is given by, $\beta = \kappa j_{\text{out}} = \kappa P\Delta c$, where κ

118   is the pumping cost. On the other hand, energy for this active transport process comes from

119   nutrients released by dying cells. If the death of a cell yields α nutrients that are divided up equally

120   among all N viable bacteria, and $-\dot{N}$ are dying per unit time, then the rate at which a bacterium is

121   supplied with nutrients is $-\alpha\,\dot{N}/N = \alpha\gamma$, where γ is the death rate. In nutrient-recycling steady-

122   state, $\dot{v} = 0$, nutrient supply and nutrient demand balance, so $\alpha\gamma = \beta$ and we obtain a quantitative

123   relation for the death rate as a function of permeability, ion gradient and the recycling yield
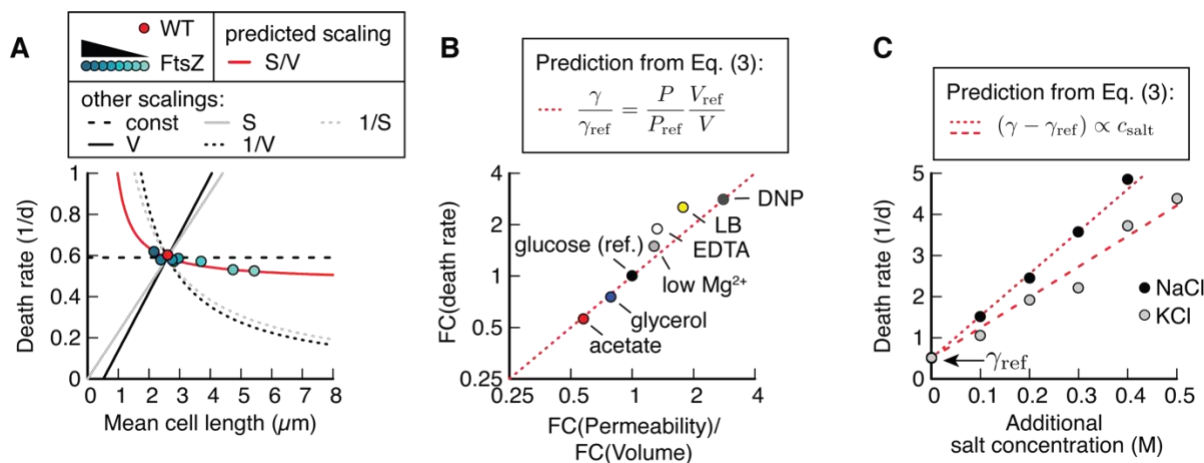
Figure 3. Cost of ion homeostasis determines death rate. (**A**) Death rate of wild-type and mutant ptac-ftsZ[27], induced with varying levels of IPTG, resulting in a change in cell length (Fig. S6). Change of death rate compared to the predicted S/V scaling, and proportional or inverse scaling with either S or V. (**B**) Fold-change (FC) of death rate, measured in batch cultures plotted versus fold-change of mean permeability (Methods) times the inverse fold change of volume, both measured in time-lapse microscopy. Theoretical prediction: Unity line in dashed red. Reference condition: growth in minimal medium with glucose (black). Red, blue: supplemented with different carbon substrates (acetate or glycerol) during growth. Light-grey: Mg^{2+} is changed during starvation from 0.4 mM to 0.1 mM. White: 1 mM EDTA added in starvation. Yellow: Growth on LB. Dark-grey: 1 mM DNP (di-nitrophenol) added in starvation. Death rates are measured as average of n=3. Permeability and volume changes are the average of 2.000 to 20.000 individual bacteria. (**C**) Death rate of cultures supplemented with either KCl or NaCl during starvation. Fit: $R^2 = 0.99$ (NaCl), $R^2 = 0.96$ (KCl).

$$\gamma = \frac{\kappa P \Delta c}{\alpha}. \tag{3}$$

124 In addition, in this simplified one-ion model, we assume that viable bacteria keep c_{in} low and
125 independent of c_{out} and P, based on the observation that bacteria keep concentrations of unwanted
126 ions low in a wide range of media, and balance osmotic pressure primarily with glutamate and
127 potassium[28].

128

129 Eq. (3) makes predictions about how lifespan should scale with cell size. Permeability P is
130 proportional to the cell surface area S, because diffusion happens across the cell membrane, while
131 the recycling yield α is proportional to cell volume V, because bigger cells release more nutrients[20].
132 Thus, according to Eq. (3), death rate should scale with the surface-to-volume ratio of bacteria,

133     $\gamma \propto S/V$, if all other factors are kept constant. There are plausible alternative hypotheses for the

134   reasons for cell death that would result in markedly different scaling. For example, if death was

135   caused by a single, rare catastrophic event, such as damage of the cell membrane or accumulation

136   of a toxic protein aggregate, death would be more likely for larger cells. Thus, we would expect

137   scaling of death rate to be proportional to membrane material, $\gamma \propto S$, or cytoplasmic material, $\gamma \propto$

138   V. On the other hand, if death is caused by a gradual deterioration of either the cell's membrane or

139   its cytoplasmic material, a bigger cell would survive longer and death rate would decrease

140   proportional either to the inverse of membrane material, $\gamma \propto S^{-1}$, or to the inverse of the total

141   cytoplasmic material, $\gamma \propto V^{-1}$.

142

143   To test whether these alternatives are better explanations of cell death during survival than our ion

144   homeostasis model, we varied cell length of *E. coli* using a titratable expression construct of the

145   cell division protein FtsZ[29] (Fig. S6). Remarkably, we observed an almost constant death rate,

146   despite a 2.5-fold variation in average length (Fig. 3A) that is clearly incompatible with the scaling

147   expected from the alternative models (black lines). Moreover, FtsZ-deprived cells also typically

148   contain several copies of chromosomal DNA[30], which suggests that DNA damage is unlikely to

149   be the death mechanism. Instead, the slight decrease of death rate in longer cells closely matches

150   the estimated surface-to-volume ratio of rod-shaped bacteria, precisely as predicted by Eq. (3) (Fig.

151   3A, red line).

152

153   To further investigate the ion homeostasis model's predictions, we wondered if differences in death

154   rates that are observed when bacteria are grown in different conditions could be explained by Eq.

155   (3). Different growth conditions prior to starvation are known to affect maintenance rate for

156   unknown reasons[20]. These changes in death rate are not accounted for by a change in S/V because

157   S/V decreases for faster growth (because cells become bigger), while death rate increases. Based

158   on Eq. (3), we suspected that these changes in death rate might instead be caused by changes in

159   bacterial permeability. To test this, we cultured *E. coli* in different growth media, washed them

160   and resuspended them in carbon free medium. From Eq. (3), the fold change (FC) of death rate

161   should be reflected in the fold changes of permeability and volume, $\mathrm{FC}(\gamma) = \mathrm{FC}(P)\,\mathrm{FC}^{-1}(V)$.

162   Indeed, quantifying average permeability for these starvation conditions, using the slope of PI

163   staining (Fig. 1F) between 0 and 10 h, showed that the change of death rate in slow-growth carbons
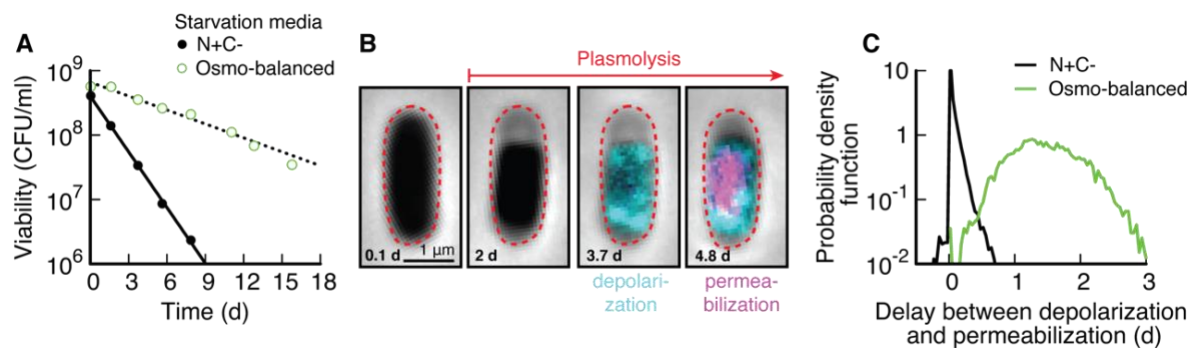
8

Figure 4. Rescued survival dynamics in 'osmo-balanced' medium. (**A**) Comparison of viability (batch) of cultures grown in N+C+ and starved in either N+C- (black, data from Fig. 1A.) or 'osmo-balanced' medium (green). Death rate decreased 4.0-fold. n=3. (**B**) Time-lapse images of *E. coli* in 'osmo-balanced' medium. After depolarization, the cytoplasm does not swell and the bacterium does not lyse. (**C**) Delay distribution between depolarization and permeabilization. In N+C- medium ('black') both events are in rapid succession, while in 'osmo-balanced' medium ('green') the events are disconnected by 1.5±0.5 days. In addition, in the 'osmo-balanced' medium both depolarization and permeabilization are gradual (Fig. S8), compared to the rapid rate of both processes in N+C- (Fig. S4). N+C-: 14.498 Osmo-balanced: 11.023 bacteria.

164 and rich media could be explained solely by the effect on permeability and volume (Fig. 3B). To

165 further test the causality of the effect of permeability on death rate, we permeabilized *E. coli* with

166 low Mg^{2+}, EDTA or DNP. These higher permeabilities were reflected in faster death rates (Fig.

167 3B). Death rates for all experimental conditions closely followed the model prediction of Eq. (3)

168 (Fig. 3B, identity line in red).

169

170 Finally, the ion homeostasis maintenance model makes the prediction that death rate should

171 depend on the medium composition. According to Eq. (3) increasing the external ion concentration

172 c_{out} should linearly increase death rate because an increase in ion gradients leads to an increase in

173 diffusive influx, which needs to be balanced with a higher pumping rate to keep the internal ion

174 concentration low. Indeed, as predicted, supplementing the medium with either NaCl or KCl led

175 to a striking linear increase in death rate, up to a 10-fold increase at 0.5 M for both salts (Fig. 3C).

176

177 For a final test, we asked if it would be possible to reduce death rates by lowering salt

178 concentrations in the medium. Consistent with our earlier observations, decreasing the

179 concentration of our phosphate-buffered minimal medium (N+C-) decreased death rate, but only

180 by about a third, before increasing again at low osmolarity (Fig. S7). This can easily be understood

181 by considering that a minimum level of external osmotic pressure is crucial to balance the internal

182 osmotic pressure from metabolites, biomolecules and cellular counterions, in order to prevent cell

183 swelling.

184

185 Guided by our model, we reasoned that it should be possible to overcome this limitation of cell

186 survival in low-salt medium by balancing cellular osmotic pressure with external osmotic pressure

187 from an impermeable osmolyte. The low-salt medium should minimize the energy cost required

188 to pump out ions, while the cellular osmotic pressure would be balanced by an external osmolyte

189 to prevent lysis. We therefore devised a new 'osmo-balanced' medium that consists of 0.2 M

190 MOPS, an inert and impermeable buffer molecule, and low quantities of essential ions; see

191 Methods. We grew *E. coli* in our regular medium to ensure an identical cell state before starvation,

192 then washed and resuspended the bacteria in the 'osmo-balanced' medium. Remarkably, this

193 medium led to a 4-fold decrease in death rate compared to our regular culture conditions (Fig. 4A).

194 This improvement of survival was not unique to *E. coli;* other bacterial species showed similarly

195 improved starvation survival in our osmo-balanced medium (Fig. S1C&D). Together, the findings

196 in Fig. 4A and Fig. 3C demonstrate that starvation survival can be controlled across a more than

197 40-fold range of death rate, simply by changing medium salt concentrations.

198

199 To confirm that our 'osmo-balanced' medium prevented cytoplasmic swelling, we performed live-

200 imaging of *E. coli*. Several days into starvation, bacteria began to depolarize, presumably due to

201 lack of energy. However, depolarized bacteria remained in plasmolysis and did not swell and lyse

202 (Fig. 4B). Most bacteria eventually permeabilized, but only several days after the loss of membrane

203 potential, as opposed to the two events coinciding, as occurred in our regular culture medium (Fig.

204 4C). Depolarization and permeabilization happened gradually (Fig. S8) rather than abruptly as in

205 regular minimal medium (Fig. S4). Thus, the osmo-balanced medium disrupted the normal death

206 process and decoupled depolarization from osmotic swelling and lysis. Unsurprisingly, bacteria

207 did not survive indefinitely in the osmo-balanced medium, which indicates that while ion

208 homeostasis is the major energy-consuming process in starvation, secondary processes also play a

209 role in survival, for example membrane turnover (see Fig. 1B).

210

211 Our results show that maintenance of ion homeostasis is the major energetic cost limiting bacterial
212 survival in starvation. Moreover, failure of ion homeostasis, triggered by a lack of energy, is the
213 cause of death of starving bacteria. The ion homeostasis maintenance model introduced here
214 explains how the stochastic exponential survival dynamics of single bacteria during starvation
215 emerge from the collective phenomena of maintenance and nutrient exchange. The model enables
216 quantitative predictions of how survival rates are affected by diverse environmental conditions and
217 bacterial adaptations. Based on our findings, we propose that targeting ion homeostasis could be a
218 promising avenue for developing novel antibiotics against non-growing and dormant infections,
219 for which currently available antibiotics are often ineffective. Finally, because most microbes on
220 earth spend most of their time in starvation conditions, we expect the principles underlying
221 starvation survival elucidated in this work, to be of broad relevance for understanding the
222 evolutionary strategies that contribute to the striking diversity of phenotypes of microbes and
223 microbial communities in different natural ecological niches.

224

Acknowledgements

234

Data availability

236 All analyzed data are available in the supporting information. Raw microscopy data can be shared
237 upon request.

238

Contributions

240 SJS and MB conceived this study, designed experiments and theory. SJS performed the majority
241 of experiments with contributions from MP in starvation experiments and microscopy, and AM in

242   electron microscopy and QPM imaging experiments. SJS, EA and MB performed modelling. SO

243   contributed to the QPM instrumentation and SO and XL designed the QPM image processing

244   pipeline. YFC constructed strains. CA contributed data analysis and ideas on membrane integrity.

245   SJS and MB wrote the paper with input from MP, AM, EA, CA, XL & SO.

246

247   **Methods**

248   *Strains*

249   All strains used in this study are derived from wild type *E. coli* K-12 strain NCM3722[31]. To titrated

250   FtsZ, the construct ptac::FtsZ of strain VIP205[29] was transferred to NCM3722 via P1 transduction.

251   Bacteria used in Fig. S1 are environmental isolates kindly provided by the lab of Roberto Kolter.

252

253   *Culture medium*

254   In this work we used two distinct culture media. Our standard medium was N-C- minimal

255   medium[32], containing K2SO4 (1 g), K2HPO4·3H2O (17.7 g), KH2PO4 (4.7 g), MgSO4·7H2O

256   (0.1 g) and NaCl (2.5 g) per liter. The medium was supplemented with 20 mM NH4Cl, as nitrogen

257   source, and 0.1% glucose as the sole carbon source, unless indicated otherwise. For carbon or

258   nitrogen starvation, N-C- minimal medium was prepared either without carbon (N+C-) or nitrogen

259   supplement (N-C+), respectively. The second medium is our 'osmo-balanced' medium, which

260   contains 0.2 M MOPS (3-(N-morpholino)propanesulfonic acid), titrated to pH 7 with KOH, and 1

261   mM $MgCl_2$, 0.1 mM $CaCl_2$, 0.16 mM K_2SO_4, 0.5 mM K_2HPO_4, 22mM NH4Cl and lacks a carbon

262   source. Cultures starved in the 'osmo-balanced' medium were previously grown in N-C- medium

263   supplemented with NH4Cl and glucose.

264

265   *Growth protocol*

266   Growth was performed in batch cultures in glass test tubes (Fisher Scientific) with disposable,

267   polypropylene Kim-Kap closures (Kimble Chase) in a water bath shaker kept at 37ºC. Single

268   colonies were picked from an LB agar plate, grown in LB until saturation and used to inoculate

269   overnight cultures in N-C- minimal media supplemented with NH4Cl and glucose. Dilutions were

270   chosen such that cultures did not saturate overnight to ensure continuous exponential growth. The

271   next day, cultures were diluted into fresh minimal medium and grown for at least 5 doublings.

272   Starvation was induced by centrifugation (5000 RCF for 3 min), removal of supernatant and

12

273   resuspension in fresh, carbon-free N-C- minimal medium or 'osmo-balanced' medium. This

274   protocol was chosen to avoid bacteria using waste products such as acetate after glucose was

275   depleted[33]. For nutrient sources without acetate excretion (e.g. glycerol), this washing step does

276   not alter the survival kinetics[17]. To achieve 'stationary phase' adaptation we used the effect of

277   excreted waste products and let *E. coli* grow on glucose until depletion, followed by washing 12 h

278   to 24 h later.

279

280   *Viability counting*

281   Samples were diluted in fresh N-C- minimal medium without carbon substrate to an estimated

282   target density of 4000 CFU/ml using a multi-channel pipette and a 96 well plate. 100 µl of the

283   diluted culture were spread on LB Agar using Rattler Plating Beads (Zymo Research) and

284   incubated for 24 h. LB Agar was supplemented with 25 µg/ml of 2,3,5-triphenyltetrazolium

285   chloride to stain colonies red and increase contrast for automated colony counting using an

286   automated CellProfiler pipeline[34]. Images were taken on a Rebel T3i (Canon) mounted on top of

287   a Lightpad A920 (Artograph).

288

289   *Live-cell Microscopy*

290   To image individual bacteria for seven days, we designed a 'no-flow' chamber that minimizes

291   nutrient contamination and evaporation. The chamber consists of a sandwich of a cover slip (22x50

292   mm, No 1.5, VWR) and a microscope slide (3"x1"x1mm, VistaVision, VWR), with a thin layer

293   of PDMS in-between. At the top and bottom, the culture is in contact with inert glass that prevents

294   evaporation or leakage of nutrients from the plastic. Two holes are laser-cut into the microscope

295   slide (Universal Laser Systems PLS 6.150D) through which the chamber will be filled. The PDMS

296   layer (Sylgard 184, 1:10 ratio, Dow Corning) is spin coated on a silicon wafer for 30 s at 500 rpm

297   (Laurell, WS-650MZ-23NPPB), cured at 85ºC for 1 h, peeled off and gently draped over the

298   microscope slide. Then, the incubation chamber is cut out of the PDMS with a laser cutter and

299   unwanted PDMS pieces are removed from the microscope slide with tweezers. The resulting

300   microscope slide with PDMS chamber is plasma treated 50 W, 10 s, O_2, duty ratio 255 (Tergeo

301   Plasma Cleaner, Pie Scientific) and the cover slide is added on top. The finished chamber is cured

302   overnight at 85ºC.

303

304   Cultures taken from exponential growth at OD 0.5 are starved according to the above protocol and

305   stained with 5 µg/ml DiBac3(4) and 1.25 µg/ml Propidium Iodide (Thermo Fisher Scientific) 10

306   minutes after entry to starvation. The 'no-flow' chamber was then filled with the stained, starved

307   culture through the laser-cut holes with a starved culture at OD 0.5, identical to batch experiments.

308   Holes are then sealed (AlumaSeal, Sigma-Aldrich) and the chamber is centrifuged, cover slide side

309   down at 1200 RCF for 2 min, to adhere bacteria to the cover glass. The majority of bacteria stably

310   adhered to the glass surface for seven days without coating. Apart from the filling and

311   centrifugation period, which were at room temperature, the culture and chamber were kept at 37ºC

312   throughout the process.

313

314   Phase contrast and fluorescence microscopy was performed on a Nikon Ti-2 equipped with a 100×

315   phase contrast immersion oil objective, Hamamatsu Flash 4.0 sCMOS camera, Lumencor Spectra-

316   X light engine and OkoLab cage microscope incubator set to 37ºC. To image the time-lapse, Nikon

317   Elements was used to control illumination times (phase: 200ms, green 10 ms, red 10 ms.) and

318   illumination strength (phase: 100%, green 10%, red 10%). A combination of perfect focus, a z-

319   stack (4 steps of 0.4 µm) and a software autofocus (post-acquisition) were used to obtain

320   continuous images of bacteria in focus.

321

322   Single cell dry mass was measured using quantitative phase microscopy (QPM) on a Nikon Eclipse

323   Ti with a Nikon, CFI Plan Apo Lambda 100X objective with 1.5 N.A. an 2x magnifier lens

324   (Thorlabs, EX2C extender) and a commercial phase sensor (Phasics, SID4bio). In the trans-

325   illumination light path, a colored-glass bandpass filter (FGB39, Thorlabs) was mounted to select

326   the blue light in order to increase the spatial resolution. This phase sensor enables single-shot

327   acquisition of quantitative phase through quadriwave lateral shearing interferometry (QWLSI)[35]

328   by using a 2-dimensional diffraction grating (modified Hartmann mask) positioned at a short

329   distance from a CCD sensor. The raw image of quantitative phase, measured as optical path

330   difference (OPD), is induced by both the sample and the optical system itself. We used the ceQPM

331   method as reported previously[36] to obtain the OPD of the optical system and fit the background

332   fluctuation that are then subtracted from the raw image to obtain the OPD of the cell. The dry mass

333   m is computed from the cell's OPD through the relation $m = 1/\alpha \cdot \oint \text{OPD}(x, y)\mathrm{d}x\mathrm{d}y$, where $\alpha =$

334    $\mathrm{d}n/\mathrm{d}c$ is the average refractive index increment of cellular materials and the integral is over the

335   cell area S. We used $\alpha = 0.18$ ml/g to convert the OPD to dry mass, which is the typical value for

336   most cellular materials[37].

337

338   Time-lapse was analyzed in MATLAB. First, regions of interests (ROIs) with an object in phase

339   contrast resembling a bacterium were identified. Next, for every time-point, the correct focal plane

340   was identified, the fluorescence background was subtracted, and the ROIs were cut out and saved

341   separately. Finally, ROIs were analyzed and the total fluorescence (by summing up the value of

342   all pixels), as well as length, width and area of the individual bacteria were recorded. For QPM

343   analysis, the segmented bacterium was dilated and the total phase-shift was integrated to yield the

344   total biomass. This analysis yielded 14,500 single-cell time-traces of bacteria starving in N-C-

345   medium (Fig. 1) and 11,000 for the 'osmo-balanced' medium (Fig. 4).

346

347   *Scanning electron microscopy protocol*

348   Culture was harvested by filtering 2 ml of exponentially growing or starving bacterial culture at

349   0.5 OD through a 0.22-micron filter (Durapore 0.22 μM PVDF membrane, Millipore

350   GVWP02500) held on a vacuum micro-filtration device (25mm glass filter holder, Millipore

351   XX1012502). Immediately after this step, the filter was submerged in Karnovsky fixative

352   (Electron microscopy sciences 15732-10). Cells were dislodged from the filter by repeated but

353   gentle pipetting with 1 ml pipette and kept in fixative solution for 1 hour at room temperature.

354   After one hour, 500 ul of fixative containing cells were added on 12 mm glass coverslip kept on a

355   35mm petri plate (glass coverslips were precoated with Ploy-L-Lysine) and centrifuged in a swing

356   bucket centrifuge (Eppendorf) for 10 min at 5000 g. After centrifugation, the glass coverslips with

357   adherent cells were placed in histology tissue fixation and processing cassettes (electron

358   microscopy sciences) and the cassettes were sequentially dipped in graded series of ethanol (30%,

359   50%, 75%, 80%, 90%, 95% and 100%). Grades of ethanol were prepared using anhydrous ethanol,

360   200 proof obtained from electron microscopy sciences (15058). Cells were kept in each grade of

361   ethanol for 10 min, and the 100% ethanol step was repeated three times with fresh ethanol to ensure

362   perfect dehydration. After this step cells were kept submerged in 100% ethanol overnight (at 4ºC)

363   and taken to Harvard center for nanoscale systems (CNS) next morning for further processing.

364   Prior to microscopy, cells were critical point dried in a Tousimis critical point dryer, mounted on

365   SEM sample holder and coated with heavy metal (gold/palladium) using sputter coater (Hummer)

366 and imaged in JEOL 5600 LV scanning electron microscope. Processing steps at CNS and imaging

367 was aided by the CNS stuff and facility in charge.

368

369 *Transmission electron microscopy protocol*

370 For transmission electron microscopy, bacterial cell samples were collected similarly as scanning

371 electron microscopy method. Briefly, 2 ml of bacterial culture at 0.5 OD was taken and cells were

372 harvested by filtration. Filter containing harvested cells were immediately dipped in Karnovsky

373 fixative, and cells were dislodged from filter by gentle pipetting. Cells in fixative were taken to

374 CNS for further processing. At CNS, cells in fixative were centrifuged to obtain a cell pellet, and

375 the pellet was embedded in resin and thin sections were prepared. Cut sections were mounted on

376 EM grid and imaged using HT7800 Hitachi TEM system.

377

378 *Quantification of permeability*

379 Live-cell microscopy with propidium iodide staining, as described see above, was used to measure

380 single-cell permeability. Fluorescence signal was integrated over the entire area of each cell, as

381 identified by thresholding in phase contrast, to calculate the total PI staining per cell of each cell

382 per time-point. PI staining rate of each cell was fitted as a direct proportionality in the period from

383 0 to 10 h to calculate the total permeability across the membrane. To calculate the change of

384 permeability compared to the reference condition, we used a 'no-flow' chamber with 6 parallel

385 channels, that allows us to measure permeability of five conditions and the reference condition in

386 the same experiment.

387

388 *Quantification of single-cell parameters*

389 To quantify plasmolysis, the threshold for segmentation of the bacterium was chosen such that it

390 contains only the cytoplasm (dark area). To quantify the length of the cell envelope, the threshold

391 was increased, such that the cell envelope (light grey are) was included in the segmentation. Both

392 thresholding techniques are semi-quantitative, as the exact boundary of the outer and inner

393 membrane cannot be resolved with phase microscopy, but they circumvent the problems generated

394 by potentially toxic membrane stains.

395

396   The Fluorescence signal from DiBac3(4) and propidium iodide was integrated over the entire
397   segmented bacterium and normalized to the cell area to correct for differences in cell size. The
398   time-point of depolarization and permeabilization was determined by the first time the signal
399   reached a threshold. For depolarization, the threshold was chosen to be the local minimum of the
400   bimodal histogram of DiBac3(4) signals of all cells throughout seven days of starvation. For
401   propidium iodide, the threshold was chosen manually. The threshold is indicated in the example
402   dynamics of individual cells in Fig. S4 and S8.

403

404   To align single-cell stretching and biomass loss, we searched in the vicinity of the time-point of
405   depolarization for the largest increase in length and the largest decrease in biomass, respectively.
406   The time delay between the time-point of depolarization and the time-points of stretching and
407   biomass loss is reported in Fig. S2.

408

409   *Cell size*

410   Cell volume was computed as $V = \pi(w/2)^2(l-w) + 4/3\,\pi(w/2)^3$ where w and l are width
411   and length of each cell, whose shape was considered as a cylinder (with radius $w/2$ and height
412   equal to $(l-w)$) with two semi-spheres at the ends (with radius $w/2$). Surface area was calculated
413   analogously as $S = 4\pi(w/2)^2 + w/2\,(l-w)$. Because cell width only changes marginally in the
414   FtsZ titration, we assumed it to be constant and took the formulas of S and V at wild-type width to
415   plot the length dependence of surface and volume in Fig. 3.

416

17

References

1. Stevenson, L. H. A case for bacterial dormancy in aquatic systems. *Microb Ecol* **4**, 127–133 (1977).

2. Amy, P. S. & Morita, R. Y. Starvation-Survival Patterns of Sixteen Freshly Isolated Open-Ocean Bacteria. *Applied and Environmental Microbiology* **45**, 1109–1115 (1983).

3. Siegele, D. A. & Kolter, R. Life after log. *J Bacteriol* **174**, 345–348 (1992).

4. De Nobili, M., Contin, M., Mondini, C. & Brookes, P. C. Soil microbial biomass is triggered into activity by trace amounts of substrate. *Soil Biology and Biochemistry* **33**, 1163–1170 (2001).

5. Hoehler, T. M. & Jørgensen, B. B. Microbial life under extreme energy limitation. *Nat Rev Microbiol* **11**, 83–94 (2013).

6. Reese, A. T. *et al.* Microbial nitrogen limitation in the mammalian large intestine. *Nat Microbiol* **3**, 1441–1450 (2018).

7. Lange, R. & Hengge-Aronis, R. Identification of a central regulator of stationary-phase gene expression in Escherichia coli. *Molecular Microbiology* **5**, 49–59 (1991).

8. Farewell, A., Diez, A. A., DiRusso, C. C. & Nyström, T. Role of the Escherichia coli FadR regulator in stasis survival and growth phase-dependent expression of the uspA, fad, and fab genes. *J Bacteriol* **178**, 6443–6450 (1996).

9. Reeve, C. A., Bockman, A. T. & Matin, A. Role of protein degradation in the survival of carbon-starved Escherichia coli and Salmonella typhimurium. *Journal of Bacteriology* **157**, 758–763 (1984).

438 10. Almirón, M., Link, A. J., Furlong, D. & Kolter, R. A novel DNA-binding protein with regulatory

439   and protective roles in starved Escherichia coli. *Genes Dev* **6**, 2646–2654 (1992).

440 11. Finkel, S. E. Long-term survival during stationary phase: evolution and the GASP phenotype.

441   *Nat Rev Microbiol* **4**, 113–120 (2006).

442 12. Gefen, O., Fridman, O., Ronin, I. & Balaban, N. Q. Direct observation of single stationary-

443   phase bacteria reveals a surprisingly long period of constant protein production activity.

444   *PNAS* **111**, 556–561 (2014).

445 13. Basta, D. W., Bergkessel, M. & Newman, D. K. Identification of Fitness Determinants during

446   Energy-Limited Growth Arrest in Pseudomonas aeruginosa. *mBio* **8**, e01170-17 (2017).

447 14. Wilson, G. S. & Topley, W. W. C. *The principles of bacteriology and immunity*. (W. Wood &

448   company, 1929).

449 15. Gay, F. P. *Agents of disease and host resistance*. (1935).

450 16. Steinhaus, E. A. & Birkeland, J. M. Studies on the Life and Death of Bacteria. *J Bacteriol* **38**,

451   249–261 (1939).

452 17. Schink, S. J., Biselli, E., Ammar, C. & Gerland, U. Death Rate of E. coli during Starvation Is Set

453   by Maintenance Cost and Biomass Recycling. *Cell Systems* **9**, 64-73.e3 (2019).

454 18. Reeve, C. A., Amy, P. S. & Matin, A. Role of protein synthesis in the survival of carbon-

455   starved Escherichia coli K-12. *Journal of Bacteriology* **160**, 1041–1046 (1984).

456 19. Phaiboun, A., Zhang, Y., Park, B. & Kim, M. Survival Kinetics of Starving Bacteria Is Biphasic

457   and Density-Dependent. *PLOS Computational Biology* **11**, e1004198 (2015).

458   20. Biselli, E., Schink, S. J. & Gerland, U. Slower growth of Escherichia coli leads to longer

459   survival in carbon starvation due to a decrease in the maintenance rate. *Molecular Systems*

460   *Biology* **16**, e9478 (2020).

461   21. Shi, H. *et al.* Starvation induces shrinkage of the bacterial cytoplasm. *Proc Natl Acad Sci USA*

462   **118**, e2104686118 (2021).

463   22. Alberts, B. *et al. Molecular Biology of the Cell*. (Garland Science, 2002).

464   23. Chang, R. *Physical Chemistry for the Chemical and Biological Sciences*. (University Science

465   Books, 2000).

466   24. Johnson, R. M. Membrane stress increases cation permeability in red cells. *Biophysical*

467   *Journal* **67**, 1876–1881 (1994).

468   25. Geddes, D. M., Cargill, R. S. & LaPlaca, M. C. Mechanical Stretch to Neurons Results in a

469   Strain Rate and Magnitude-Dependent Increase in Plasma Membrane Permeability. *Journal*

470   *of Neurotrauma* **20**, 1039–1049 (2003).

471   26. Slomka, N. & Gefen, A. Relationship Between Strain Levels and Permeability of the Plasma

472   Membrane in Statically Stretched Myoblasts. *Ann Biomed Eng* **40**, 606–618 (2012).

473   27. Kramers, H. A. Brownian motion in a field of force and the diffusion model of chemical

474   reactions. *Physica* **7**, 284–304 (1940).

475   28. Richey, B. *et al.* Variability of the intracellular ionic environment of Escherichia coli.

476   Differences between in vitro and in vivo effects of ion concentrations on protein-DNA

477   interactions and gene expression. *Journal of Biological Chemistry* **262**, 7157–7164 (1987).

478   29. Palacios, P., Vicente, M. & Sánchez, M. Dependency of Escherichia coli cell-division size, and

479   independency of nucleoid segregation on the mode and level of ftsZ expression. *Mol*

480   *Microbiol* **20**, 1093–1098 (1996).

481   30. Sánchez-Gorostiaga, A. *et al.* Life without Division: Physiology of Escherichia coli FtsZ-

482   Deprived Filaments. *mBio* **7**, e01620-16 (2016).

483   31. Soupene, E. *et al.* Physiological Studies of Escherichia coli Strain MG1655: Growth Defects

484   and Apparent Cross-Regulation of Gene Expression. *J Bacteriol* **185**, 5611–5626 (2003).

485   32. Csonka, L. N., Ikeda, T. P., Fletcher, S. A. & Kustu, S. The accumulation of glutamate is

486   necessary for optimal growth of Salmonella typhimurium in media of high osmolality but

487   not induction of the proU operon. *Journal of Bacteriology* **176**, 6324–6333 (1994).

488   33. Basan, M. *et al.* Overflow metabolism in Escherichia coli results from efficient proteome

489   allocation. *Nature* **528**, 99–104 (2015).

490   34. Carpenter, A. E. *et al.* CellProfiler: image analysis software for identifying and quantifying

491   cell phenotypes. *Genome Biol* **7**, R100 (2006).

492   35. Bon, P., Maucort, G., Wattellier, B. & Monneret, S. Quadriwave lateral shearing

493   interferometry for quantitative phase microscopy of living cells. *Opt Express* **17**, 13080–

494   13094 (2009).

495   36. Liu, X., Oh, S., Peshkin, L. & Kirschner, M. W. Computationally enhanced quantitative phase

496   microscopy reveals autonomous oscillations in mammalian cell growth. *Proc Natl Acad Sci U*

497   *S A* **117**, 27388–27399 (2020).

498   37. Barer, R. & Joseph, S. Refractometry of Living Cells : Part I. Basic Principles. *Journal of Cell*

499   *Science* **s3-95**, 399–423 (1954).